In-vitro validation of some flow assumptions for the prediction of the pressure distribution during obstructive sleep apnea

A. Van Hirtum[a*], X. Pelorson[a], and P.Y. Lagrée[b].

[a]Institut de la Communication Parlée,

UMR CNRS 5009, INPG-Université Stendhal,

46 Av. Félix Viallet, 38031 Grenoble, France

[b]Laboratoire de Modélisation en Mécanique,

UMR CNRS 7607, Université Paris VI,

4 Place Jussieu, Tour 66, case 162,

75252 Paris, France

Keywords: upper airway collapse, obstructive sleep apnea syndrome, pressure distribution, tongue replica, geometrical asymmetry, flow separation postition, boundary layer solution, Reduced Navier Stokes

short title = in-vitro study of OSA

*corresponding author: e-mail: annemie@icp.inpg.fr, fax: (33) 4 76 57 47 10

An adequate description of the pressure distribution exerted by the fluid flow on pharyngeal walls is a first requirement to enhance the understanding, modelling and consequently the prediction of airway collapse during obstructive sleep apnea. From a fluid mechanical point of view several flow assumptions can be formulated to reduce the governing flow equations. The relevance of some major flow assumptions and the accuracy of the resulting flow description with respect to obstructive sleep apnea is investigated on a rigid geometrical replica of the pharynx. Special attention is given to the influence of geometrical asymmetry and to the position of the flow separation point. An 'in-vitro' experimental and theoretical study of steady pharyngeal fluid flow is presented for different constriction heights and upstream pressures. Pressure and velocity distributions along a rigid 'in-vitro' replica of the oro-pharyngeal cavity are compared with different flow predictions based on various assumptions. Fluid flow models are tested for volume flow rates ranging from 5 up to 120l/min and for minimum apertures between 1.45 and 3.00mm. Two dimensional flow models are required and predict experimental results within an accuracy of 15%. Flow theories classically used in the case of a Starling resistor provide a poor agreement.

1. INTRODUCTION

Obstructive sleep apnea (OSA) is defined as the intermittent cessation of breathing during sleep and is characterised by recurrent collapse of the pharyngeal airway. OSA is extensively shown to be an important health care issue with a reported prevalence of 4 % in adult men and 2 % in adult woman (YOUNG et al. 1993). OSA causes excessive daily sleepiness and increases the development of cardiovascular diseases and arterial hypertension (PEPPARD et al. 2000). Consequently OSA has adverse consequences on the patients daily life and is associated with an increased risk on public traffic accidents (FLEMONS and REIMER 2002, TERAN-SANTOS et al. 1999).

The OSA syndrome is mainly treated using empirical therapeutical or surgical procedures. Long-term use of therapeutical treatment strategies like continuous positive airway pressure or pharyngeal appliances cause daily discomfort and as such reduces the quality of life (FLEMONS 2002). The long-term effectiveness of surgical treatment is estimated to range between 50 and 78 % depending on the applied surgical procedure (FLEMONS 2002, BRIDGMAN and DUNN 2002, SHER et al. 1996). Therefore current research aims to improve diagnosis, follow-up and treatment of the OSA syndrome. In particular the need for further understanding of the OSA syndrome in order to favour successful development of therapeutical and surgical treatments is stressed (FLEMONS 2002, HUI et al. 2000, LIPTON and GOZAL 2003, MCNICHOLAS 2003, PENZEL et al. 2002, RAMA et al. 2002, AYAPPA and RAPOPORT 2003, PAYAN et al. 2002). The present study is an essential step towards a physical model of the ongoing flow phenomena. A physical flow model is a first requirement to model the fluid/structure interactions at longterm aiming to predict the outcome of surgical interventions.

The upper airway is a potentially collapsible structure whose patency is dictated by a combination of passive mechanical properties and active neural mechanisms. In particular the OSA syndrome is known to be due to a partial (hypopnea) or total (apnea) collapse of the upper airway during inspiration (AYAPPA and RAPOPORT 2003). The Starling Resistor is a classical experiment used to study biofluid mechanical applications involving collapsible structures such as flow limitation in the airway branches (GROTBERG and JENSEN 2004, LAMBERT and WILSON 1972). Due to the pharyngeal asymmetry in both geometry and tissue properties (rigid hard palate versus soft tissues) the relevance of such devices for the study of OSA is not obvious. An alternative set-up is presented in this paper. From a physical point of view, neglecting neural mechanisms, the airway collapse is due to the fluid-mechanical interaction of the fluid (airflow during inspiration) and the surrounding structure (tissues). Studies of the biomechanical pharyngeal airflow and resulting forces in case of OSA are very limited. Because of a wide clinical interest, most of the literature in the field concentrates on the relationship between inspiratory and expiratory pressure and the volume flow velocity. Usually the pressure-flow relationship in the upper airway is mathematically fitted by a quadratic or polynomial function in order to objectively detect inspiratory flow limitation and related phenomena (HENKE 1998, MANSOUR et al. 2002). The resulting pressure-flow relationship obtained by curve fitting of the applied mathematical polynomial or quadratic formulation may provide useful empirical information, but does not describe the complexity of the ongoing physical flow behaviour and does not inform on the pharyngeal pressure distribution.

The interaction between the fluid and the surrounding upper airway tissue is expressed by the force excerted by the fluid on the surrounding tissue. This force is determined by the pressure distribution. Therefore not only the volume flow velocity needs to be accurately predicted from the upstream pressure as aimed in (HENKE 1998, MANSOUR et al. 2002), but also does the pressure distribution along the upper airway. With respect to an accurate description of the pressure distribution it is generally accepted that an accurate prediction of flow separation is crucial (MATSUZAKI and FUNG 1976, PEDLEY and LUO 1998).

A three-dimensional computational simulation of airflow characteristics, including both volume flow velocity and pressure distribution, in an anatomical accurate rigid human pharynx geometry is assessed in (SHOME et al. 1998). The airflow was assumed to be incompressible and steady. The pressure drop in the pharynx was quantified to lie in the range of 200-500Pa provoking the pharynx to collapse. The onset from laminar to turbulence flow was found to increase the pressure drop with 40 %. Subtle effects on the airway morphology, as introduced by surgical treatment of OSA, were shown to have a large effect on the pressure drop.

The presented work aims to contribute to the understanding of flow induced pharyngeal airway obstruction at the origin of OSA. The pressure distribution along an rigid 'in-vitro' geometrical constriction, representing the pharyngeal cavity, was predicted from the upstream pressure and geometrical information. Several assumptions on the flow and the constriction geometry are experimentally assessed. The model performance of corresponding flow models with increasing complexity is systematically and quantitatively validated.

2. Theory

2.1. Assumptions and dimensional numbers

From a fluid mechanical point of view several flow assumptions can be formulated on the basis of a dimensional analysis of the governing flow equations. This yields a set of non-dimensional numbers, which can be interpreted as a measure of the importance of various flow effects. Based on the obtained orders of magnitude for the characteristic non-dimensional numbers approximations are made to describe the flow. Conserning obstructive sleep apnea four non-dimensional numbers are derived based on characteristic conditions listed in Table 1. Physiological data are obtained from 'in-vivo' observations (LEITH 1995, MAYER et al. 1996, SCHWAB et al. 1990).

Firstly, the squared value of the Mach number, $Ma = \frac{U_0}{c_0}$, the ratio of flow velocity U_0 to the speed of sound c_0 indicates the tendency of the flow to compress as its encounters a solid boundary. Since the velocities involved during respiration are small compared with the speed of sound in air ($Ma_0^2 \approx O(10^{-4})$) the flow is assumed to be incompressible.

Secondly, the Strouhal number $Sr = \frac{L_0}{t_0 U_0}$, is a dimensionless frequency indicating the ratio of the distance over which flow is convected in a characteristic time t_0 over a characteristic width L_0 of a structure exposed to the flow. The airflow can be considered as primarily steady as long as the flow patterns at any given time are approximately the same, which is reasonable during quiet breathing at the characteristic respiratory frequencies and rigid walls expressed by a low Strouhal number $Sr_0 \approx O(10^{-3})$.

The assumptions of incompressible and steady flow will not be discussed in the present article. The assumptions are indeed widely accepted in the literature (GROTBERG and JENSEN 2004, PEDLEY and LUO 1998, SHOME et al. 1998). Note that in the case of snoring these assumptions would certainly be discutable.

Thirdly the Reynolds number, $Re = \frac{\rho_0 U_0 h_0}{\mu_0}$ with U_0 a typical flow velocity, h_0 a typical dimension (such as the pharyngeal minimum aperture), μ_0 the dynamic viscosity and ρ_0 the density, represents the importance of inertial forces with respect to the viscous forces acting on a given fluid element and the length of the pharyngeal replica. In first approximation the flow is assumed to be inviscid considering the involved characteristic Reynolds numbers $Re_0 \approx O(10^3)$. Although it can be neglected for the bulk of the flow, viscosity is important near the walls motivating the application of the boundary layer theory. Next, the occurence of flow separation is a consequence of the viscosity and has a strong influence on flow control (MATSUZAKI and FUNG 1976, PEDLEY and LUO 1998). Therefore the flow separation point is either considered to be fixed by an empirical 'ad-hoc' assumption or is predicted based on physical principles. The relevance of this assumption and its influence on the position of flow separation is extensively investigated in this paper.

Fourthly, the ratio of characteristic geometrical lengths yields information about the dimensionality of the flow. The aspect ratio h_0/W_0 is considered, with h_0 a typical minimum aperture and W_0 a typical width. Following the characteristic ratio $h_0/W_0 = 0.09$ $[h_0/W_0 << 1]$ the flow is assumed to be completely characterised by a bidimensional flow description in the (x,y)-plane. This assumption will be experimentally tested.

In the next subsection different flow descriptions are presented based on the assumptions with respect to viscosity, dimensionality of the flow description and to the influence of the asymmetry on the geometrical replica. As a result the flow predictions resulting from different simplifications of the bidimensional laminar, incompressible and quasi-steady Navier Stokes (NS) equations can be numerically and experimetally validated.

2.2. Theoretical flow predictions

The origin of OSA lies in a strong interaction of the fluid and the surrounding tissue provoking the pharyngeal airway recurrently to collapse during sleep. A first requirement to describe ongoing phenomena is to know the pressure variations through the pharyngeal geometry. Since an exact analytical solution for the flow through such a constriction is not available different flow models and flow assumptions are assessed to estimate 1) the volume flow velocity ϕ and 2) the pressure distribution p(x) as function of position (BLEVINS 1992, SCHLICHTING and GERSTEN 2000).

Once p(x) is known the force F(x) acting by the airflow on the surrounding tissue of the pharynx is deduced as $F(x) = \int pdS$.

2.2.1. Bernoulli with ad-hoc viscosity correction

In first approximation, the flow is assumed to be fully inviscid. The three assumptions of incompressible, quasi-steady and inviscid flow allow to apply the steady one-dimensional (1D) Bernoulli law (1),

$$p(x) + \frac{1}{2}\rho U(x)^2 = cte, \tag{1}$$

to estimate the pressure distribution p(x) along the pharyngeal walls. The volume flow velocity is defined by $\phi(x) = U(x)A(x) = cte$ with $U(x)$ the local flow velocity and $A(x)$ the area along the pharyngeal replica. To be useful, an empirical ad-hoc correction is needed to the 1-D Bernoulli equation to account for the occurrence of flow separation downstream of h_{min}. The jet formation downstream of the point of flow separation is due to very strong viscous pressure losses and reversed flow occuring near the wall and thus can not be predicted by the Bernouilli law. For a steady flow the onset of separation coinciding with the separation point is defined as $\frac{\partial U}{\partial n}|_{n=0} = 0$. In literature, the area associated with flow separation A_s is empirically chosen as 1.2 times the minimum area A_{min} along the replica, i.e. $A_s = cA_{min}$, with $c = \frac{A_s}{A_{min}} = 1.2$ (PAYAN et al. 2002, HOFMANS et al. 2003). The ad-hoc correction for the 1D Bernoulli (1) results in a steady 1D expression for $p(x)$ given in (2), with p_0 and A_0 respectively the pressure and area upstream of the replica indicated in Figure 2. The volume flow velocity is estimated as (3). In expression of (2) pressure recovery downstream of the point of flow separation is neglected.

$$p(x) = p_0 + \frac{1}{2}\rho\phi^2\left(\frac{1}{A_0^2} - \frac{1}{A(x)^2}\right) \tag{2}$$

$$\phi = A_s\sqrt{\frac{2(p_0)}{\rho}}, A_s = cA_{min} \tag{3}$$

The preceding assumption of inviscid flow is not valid for low Reynolds numbers. This is the case for low flow velocities U or/and small h_{min} values. In this case, an extra Poiseuille term is often added to the Bernoulli expression for p(x) in (2) to correct for viscous pressure losses. The Bernoulli expression with Poiseuille correction is given in (4) with μ the dynamic viscosity coefficient, D the diameter of the half cylinder and h(x) the heigth between the half cylinder and the flat plate as defined in subsection 3.1.

$$p(x) = p_0 + \frac{1}{2}\rho\phi^2\left(\frac{1}{A_0^2} - \frac{1}{A(x)^2}\right) - \frac{12\mu\phi}{D}\int\frac{dx}{h(x)^3} \tag{4}$$

2.2.2. Boundary layer solution

In the preceding subsection 2.2.1 the viscosity is either neglected (Bernoulli in (2)) or corrected with an additional Poiseuille term, assuming a fully developed Poiseuille flow

(Poiseuille in (4)). However, at high Reynolds numbers the region in which viscous forces are important is confined to a thin layer adjacent to the wall which is referred to as laminar boundary layer δ. Outside of the boundary layer, the inviscid irrotational main flow, with velocity U(x), is described by Bernoulli (3). The resulting boundary layer theory is described by the Von Kármán momentum integral equation for steady flows (SCHLICHTING and GERSTEN 2000). An approximated method to solve this equation for laminar incompressible bidimensional (x,y) boundary layers is given by Thwaites method.

Introducing two shape parameters $H(\lambda) = \frac{\delta_1}{\delta_2}$, $S(\lambda) \propto \frac{\tau_S \delta_2}{U}$ which are only functions of the velocity profile determined by the acceleration parameter $\lambda \propto \frac{dU}{dx}\delta_2$, with $\tau_S(x) \propto \lim_{n\to 0} \frac{\partial u}{\partial n}$ the wall shear stress indicating the viscous force per unit area acting at the wall, the displacement thickness δ_1

$$\delta_1(x) = \int_0^\infty \left(1 - \frac{u(y)}{U}\right) dy, \tag{5}$$

and the momentum thickness δ_2

$$\delta_2(x) = \int_0^\infty \frac{u(y)}{U} \left(1 - \frac{u(y)}{U}\right) dy. \tag{6}$$

The Von Kármán equation is then approximated by

$$\delta_2^2(x)U^6(x) - \delta_2^2(0)U^6(0) \propto \int_0^x U^5(x)dx. \tag{7}$$

Equation (7) in combination with the fitted formulas for H(λ) and S(λ) tabulated in (BLEVINS 1992) enables to compute the strived pressure distribution $p(x)$ up to the flow separation point where $\tau_S = 0$ for a given input pressure and know geometry. Moreover, the point of flow separation x_S is numerically estimated since separation is precicted to occur at $\lambda(x_S) = -0.0992$ (PELORSON et al. 1994). So no ad-hoc assumption is made to account for flow separation.

In (DEVERGE et al. 2003) the method was successfully applied to accurately predict the position of flow separation and associated pressure within the glottis. In the present study the prediction of the pressure distribution along the pharyngeal replica is assessed. Although since flow prediction downstream of the position of flow separation is not possible in the following subsections two numerical methods of flow predictions are outlined.

2.2.3. Reduced Navier Stokes

A second simplification of the Newtonian steady laminar incompressible bidimensional Navier Stokes equations is obtained making two additional assumptions. Firstly the flow is assumed to be characterised by a large Reynolds number and secondly the geometrical transverse dimension (y-axis) is assumed to be small compared to the longitudinal dimension (x-axis). In the geometry under study the last assumption coincides with $h_0 << D$. Applying those assumptions to the bidimensional NS equations results in a system in which the transverse pressure variations are neglected. This system is referred to as the Reduced Navier Stokes/Prandtl (RNSP) system in accordance with Prandtl's formulation of the steady boundary-layer. Nondimensional variables are obtained by scaling u^* with U_0, v^* with U_0/Re, x^* with $h_0 Re$, y^* with h_0 and p^* with ρU_0^2 with the Reynolds number defined as $Re = U_0 h_0/\nu$. In terms of the nondimensional variables the resulting RNSP equations become:

$$\frac{\partial}{\partial x}u + \frac{\partial}{\partial y}v = 0, \qquad u\frac{\partial}{\partial x}u + v\frac{\partial}{\partial y}u = -\frac{\partial}{\partial x}p + \frac{\partial^2}{\partial y^2}u, \qquad 0 = -\frac{\partial}{\partial y}p. \tag{8}$$

The no slip boundary condition is applied to the lower and upper wall. Since the lower wall of the geometry of interest corresponds to $y = 0$ and the distance to the upper wall is denoted with $h(x)$ the no slip condition becomes respectively $(u(x, y = 0) = 0$, $v(x, y = 0) = 0)$ and $(u(x, y = h(x)) = 0$, $v(x, y = h(x)) = 0)$. In order to numerically solve the RNSP equations the pressure at the entrance is set to zero and the first velocity profile need to be known (Poiseuille). There is no output condition.

3. Material

In order to enable experimental validation of the predicted pressure distribution for a given pressure, a suitable 'in-vitro' pharyngeal replica and experimental set-up is required.

3.1. In-vitro pharyngeal tongue replica

The place of obstruction in the pharynx at the origin of OSA is known to be very variable (naso-, oro- or laryngopharynx) (RAMA et al. 2002). Regardless the precise location of obstruction in the pharynx the relevant anatomy is 'in-vitro' imitated by a rigid half cylinder, representing roughly the tongue geometry, placed inside a rectangular uniform pipe representing thus the pharyngeal wall. Changing the minimum aperture (h_{min}) between the tongue-replica and the pipe allows the study of different anatomical conditions. Consequently the important geometrical parameters are the diameter D of the half cylinder and the value of h_{min}. In this study the diameter D of the rigid replica is fixed to 49mm which is in accordance with anatomical 'in-vivo' values. Different degrees of constriction are studied by changing h_{min} between the half cylinder and the flat plate. Minimum distances h_{min} of 1.45, 1.90, 2.30 and 3.00mm are considered. These distances were measured using calibrated plates with an accuracy of 0.01mm. In order to connect the replica to the experimental set-up described in subsection 3.2 a triangular attachment of length 25mm and heigth 6mm is fasten to the upper part of the half cylinder maintaining a fixed vertical height of h_0=34mm between the beginning of the attachment and the flat plate. A photograph and longitudinal cross-section of the resulting pharyngeal geometry constituted from the attachment and 'in-vitro' tongue replica is depicted in respectively Figure 1 and Figure 2 for the assessed h_{min}'s. The flat plate coincides with the x-axis at y=0. The changing height of the replica along the x-axis is further denoted with $h(x)$. Remark the physiologically observed strong asymmetrical nature of the replicas geometry in the (x,y)-plane. The replica has a fixed width W of 34mm along the z-dimension.

3.2. Experimental set-up

To simulate the origin of OSA the rigid pharyngeal replica is attached to an 'in-vitro' test-installation. The test-installation enables to study the influence of various incoming (inspiration) pharyngeal airflow conditions. To validate theoretical flow predictions, flow characteristics are measured at different positions along and upstream of the tongue replica. Incoming airflow conditions are determined by measuring the volume flow velocity (ϕ) and upstream pressure (p_0) as indicated in Figure 2. The volume flow velocity ϕ [l/min] is measured using a thermal mass flow meter (TSI 4040) with an accuracy of 0.01 l/min. Flow pressure measurements [Pa] are performed at three different positions (p_1, p_2, p_3) depicted in Figure 2 along the converging part of the rigid tongue replica and the flat bottom plate. The pressure is measured with piezoresistive pressure transducers

(Endevco 8507C or Kulite XCS-093) positioned in pressure taps of 0.4mm diameter at the mentioned sites which allows dynamic pressure measurements. The site p_3 corresponds to the position h_{min}. The sites p_2 and p_1 are respectively located upstream from the site p_3 at 4.5mm and 8.0mm along the x-dimension. The presure transducers are calibrated against a water manometer with an accuracy of 1 Pa. The volume flow velocity ϕ and pressure distribution p(x) along the replica are predicted from the measured upstream pressure p_0.

Next to pressure measurements a constant temperature anemometer system (IFA 300) is available in the test-installation to perform flow velocity measurements with accuracy of 0.1 m.s^{-1}. Velocity profiles can be obtained by moving the hot film using a two dimensional stage positioning system (Chuo precision industrial co. CAT-C, ALS-250-C2P and ALS-115-E1P). The accuracy of positioning in the x and y direction is respectively 4 and 2 μm.

4. Predictive performance

The performance of the distinct flow predictions defined in subsection 2.2 will be statistically quantified by the coefficient of determination R^2 ($0 \leq R^2 \leq 1$),

$$R^2 = 1 - \frac{\hat{\sigma}^2}{\sigma_y^2}, \tag{9}$$

with $\hat{\sigma}^2$ the sample variance of the prediction residuals and σ_y^2 the sample variance of the measured output about its mean value. Larger R^2 values correspond to increased predictive model performance.

5. Results and discussion

The flow predictions outlined in section 2.2 are developed assuming particular flow conditions. Therefore major flow assumptions discussed and motivated in subsection 2.1 are experimentally validated before in the following sections the predictive value of the flow descriptions is systematically explored.

5.1. Experimental validation of some major flow assumptions

5.1.1. Spatial distribution of the flow

The steady flow models presented in section 2.2 result in a 1D, quasi-2D or 2D flow description. The third dimension (z-axis) perpendicular to the (x,y) plane is assumed to have no influence on the flow. In order to validate this assumption, the horizontal velocity profile is measured for each h_{min}. Figure 3 illustrates an exemplary velocity profile for $h_{min} = 2.3mm$ and a steady flow of 60 l/min. The step Δz at the edges near the wall is 0.1 mm elsewhere Δz equals 1.0 mm. The anemometer is positioned as close as possible to the minimum aperture. The measured velocity has a standard deviation (ξ [%]) $\xi < 1\%$ around its mean value. $\xi < 1\%$ corresponds to a flat velocity profile along the z-direction. For all assessed apertures and volume flow rates $\xi < 1\%$ is maintained. At the edges, where a smaller stepsize of $\Delta z = 0.1$ mm is applied, the measured velocities are slightly decreased due to the presence of the boundary layer. Consequently neglecting the z-dimension in the flow description is positively validated and as such a bidimensional (x,y) spacial distribution of the flow is motivated.

The velocity profiles depicted following the y-dimension in figure 4 draw attention to the asymmetry of the flow within the pharyngeal replica. The vertical velocity along the y-dimension is measured while the x-value coincides with an aperture of 9mm along the diverging side of the replica. This position is indicated by the horizontal line at h(x)=y=9mm in Figure 2. The vertical velocity profile is measured with a spatial resolution of $\Delta z = 0.1$mm. Figure 4 shows the vertical velocity profile for volume flow velocities ranging from 20l/min up to 100l/min for a minimum aperture $h_{min} = 2.30mm$. y=0 corresponds with the flat plate of the replica. For high volume flow velocities the vertical velocity profiles in figure 4 becomes asymmetrical. In order to evaluate the impact of the asymmetry on the pressure distribution the pressure is measured at positions p_1, p_2 and p_3 on the half cylinder as well as on the flat bottom plate as indicated in figure 2. Figure 5 represents an example of the normalized pressure measurements for different values of the upstream pressure p_0 for the minimum aperture $h_{min} = 3.00mm$. At the position of the minimum aperture the ratio $\frac{p_3}{p_0}$ approximates -0.15 for both the pressures measured on the half cylinder as on the flat bottom plate. This ratio is of the same order of magnitude than the one mentioned in (HOFMANS et al. 2003) for a symmetrical lip replica with a comparable minimum aperture of $h_{min} = 3.36mm$. Thus at the position of minimum aperture the measured pressure difference is between the half cylinder and the flat plate is very limited. The pressures measured at the flat plate at position p_2 are by a few percent superior to the pressures measured at the half cylinder. Looking at the measurements at position p_1 the same finding holds. Furthermore the transverse pressure difference is found to decrease approaching the minimum aperture. So the influence of the asymmetry on the pressure measurements augments with increasing absolute value of the spatial derivative. Although systematically, the measured pressure gradients at positions p_2 and p_1 are far inferior to 10%, which is small compared to the general accepted error range of 25% (HOFMANS et al. 2003). Same findings hold for all assessed minimum apertures. Therefore it is concluded that although measurable, the asymmetry hardly affects transverse pressure measurements and so the strived pressure distribution p(x). This finding is important considering application of the boundary layer theory since, as expressed in equation 8, the equations of motion within the boundary layer assume that transverse pressure variations can be neglected.

5.1.2. Flow prediction

Figure 6 illustrates a detailed bidimensional velocity map for a steady flow of 40 l/min with a minimum aperture of $h_{min} = 3.00$mm. The presented findings hold for all assessed minimum apertures and volume flow velocities. The anemometer is displaced with a step of $\Delta x = 1$mm in the x direction and $\Delta y = 0.05$mm in the y direction. The same way as for the horizontal velocity profile depicted in Figure 3 the decrease in velocity towards the edges provides experimental evidence for the existence of the boundary layer. Along the diverging part of the replica the velocity tends to zero, which experimentally illustrates the impact of flow separation on the flow also mentioned in (SHOME et al. 1998). The importance of the boundary layer and flow separation on the bidimensional flow description is further illustrated in figure 4. The plotted profiles show the existence of a boundary layer near the edge ($y/h_{min} = 0$) and the formation of a jet since the velocity tends to 0 as the ratio y/h_{min} becomes superior to 1. The development of the inviscid main flow with increasing volume flow velocity is clearly illustrated. Due to the importance of the position of flow separation on the flow control in the following the relevance of the assumption with respect to a fixed or predicted flow separation point are extensively considered with respect to the strived pressure distribution.

The ad-hoc corrected Bernoulli law with the assumption of fixed flow separation point described in subsection 2.2.1 results in the most simplified prediction of the strived pressure distribution. The application of the one dimensional pressure prediction is illustrated in figure 7 for a minimum aperture $h_{min} = 1.45mm$. The volume flow velocity ϕ is varied from 5 up to 120l/min in steps of 5l/min (Re $\leq$ 4719). The ratio of the measured and upstream pressure p_0 at the positions p_1, p_2 and p_3 are indicated with crosses. The one dimensional pressure distribution p(x) is shown for two different positions of flow seperation expressed by two values of the constant $c = \frac{A_s}{A_{min}}$. The constant c is chosen to 1.2 and 1.05 corresponding to respectively the value proposed in literature and the value retrieved from the measured data $c = \sqrt{1 - \frac{p_3}{p_0}} = 1.05$. Remark that in the last case the modelling performance is optimized by using not only one input value (p_0), but two (p_0,p_3). Since p_3 is used as an input the predicted pressure values at position p_3 are expected to correspond well with the measured pressures. The origin of the OSA syndrome is qualitatively explained by the negative pressure at the level of the constriction. As expected an accurate quantitative model is obtained for the region of maximal pressure drop (R^2=0.99 at site p_3) from the 1D flow description. The impact of the 'ad-hoc' value c or the position of flow separation on the predicted pressure distribution is obvious. Consequently the position of flow separation (or the value of the constant c) will largely affect the forces excerted by the flow on the surrounding tissues. In order to further evaluate the retrieved constant $c = 1.05$ figure 9 shows the physical value of the constant c predicted using Thwaites method and RNSP. It appears that the ad-hoc value c=1.05 greatly underestimates the position of flow separation x_S for all covered volume flow velocities. So although the ad-hoc value c=1.05 optimises the 1D modeling performance it is an unphysical value resulting in a less accurate force distribution since

$$F = W \int_{inlet}^{separation} p(x)dx. \qquad (10)$$

Therefore one dimensional pressure prediction involving a fixed position of the flow separation point is not useful for application to OSA where the force distribution is important and will not be considered further. This finding is in agreement with (PEDLEY and LUO 1998, MATSUZAKI and FUNG 1976) who stresses the importance of an accurate prediction of flow separation and the need to improve the one-dimensional model with more modern boundary layer methods.

Figure 8 shows the measured and predicted longitudinal velocity profile along the x-axis using Thwaites method and RNSP, outlined in subsections 2.2.2 and 2.2.3 for a steady flow of 40 l/min with a minimum aperture $h_{min} = 3.00$mm. Note the limited range of experimental data along the longitudinal dimension, i.e. the x-axis. This is due to the physical dimensions of the hot film probe preventing further insertion inside the replica. Thwaites method doesn't allow to compute any predictions past the point of flow separation. Consequently for large x values only experimental datapoints and RNSP predictions can be seen. The same findings hold for all assessed minimum apertures and volume flow velocities.

The velocity values obtained with both Thwaites method and RNSP are within 10 % agreement with the measured velocity values. Although the velocity distribution within the replica seems much more accurate with RNSP since the trend in the measured data is captured.

5.2. Pressure distribution

The predictive value of the bidimensional flow predictions using Thwaites method and RNSP is quantitatively explored. Since the position of flow separation largly affects the force distribution, we reconsider the predicted values of the constant c for different volume flow velocities depicted in figure 9. Altough very close, the constant predicted with Thwaites is systematically superior to the constant obtained from RNSP. Consequently RNSP predictes flow separation to occur prior compared to Thwaites. Although, for all assessed minimum apertures the difference in the predicted constant is small ($< 3\%$), except for small volume flow velocities where the difference incresases up to $\pm 10\%$. To evaluate the prediction of the pressure distribution with Thwaites and RNSP the pressures measured at positions p_1, p_2 and p_3 are compared to the computed pressures. Figures 10, 11, 12, 13, 14 and 15 show the predicted and measured data normalised by the upstream pressure p_0 at positions p_1, p_2 and p_3 for respectively $h_{min} = 1.45mm$ and $h_{min} = 3.00mm$ as function of the upstram pressure p_0. In all figures the pressure drop predicted by RNSP is slightly superior to the pressure drop predicted by Thwaites method. A larger pressure drop agrees with the slightly inferior value of the constant c mentioned earlier in case of RNSP. Figures 12 and 15 illustrate that both Thwaites and RNSP pressure predictions at the minimum aperture p_3 yields well within the typically accepted error range of 25% on the measured pressure values (HOFMANS et al. 2003). From the remaining figures it can be seen that this hold also for the pressure measured at positions p_1 and p_2. Note from Figure 7 that using Bernoulli would give estimation errors far above the accepted error range of 25% in case the position of flow separation is respected (c=1.2). The overall model performance for all assessed minimum apertures (1.45, 1.90, 2.30, 3.00 mm) at the positions p_1, p_2 and p_3 for Thwaites and RNSP is detailed in Table 2. The overall model accuracy is expressed by the mean coefficient of determination R^2 defined in equation 9 averaged for all minimum apertures and the indicated ranges of volume flow velocities extending from 5 l/min to respectively ≤30, ≤60, ≤80, ≤100 and ≤120 l/min. The covered ranges allow to value the predictive value for distinct Reynolds numbers $Re = \frac{\phi}{W\nu}$, with ν being the kinematic viscosity coefficient and W and ϕ as defined previously. For all 5 cases the model performance of both Thwaites and RNSP at the position of minimum constriction $R^2_{p_3}$ is excellent ($R^2_{p_3} > 0.97$). Further it can be seen that in general $R^2_{p_1} \leq R^2_{p_2} \leq R^2_{p_3}$. So the R^2 and thus the prediction performance increases approaching the position of minimum aperture. This finding stresses the importance to validate the pessure predictions at different sites along the replica in order to compare and evaluate flow predictions if the pressure distribution is of interest. From table 2 follows the model performance significantly increases for Reynolds numbers below ±2500. Reynolds numbers below 2500 are characteristic for laminar flows. Higher values of the Reynolds number indicate the transition from laminar to turbulent or turbulent flows. Since the applied bidimensional flow predictions are laminar flow models the flow behaviour was expected to be most accurately described within the laminar range, as is the case. Furthermore the predictive value of RNSP exceeds slightly Thwaites predictions for low volume flow velocities in the laminar range. The volume flow velocities involved during OSA are below 30 l/min (FISHMAN et al. 1986). So, in case of OSA the predictive value of RNSP exceeds slightly the predictive value of Thwaites method and RNSP prediction is favoured to acquire the pressure distribution. This holds in particular for the position p_1, where the influence of the asymmetry is largest. Although it can be seen that areas with the largest pressure drop will most contribute to the origine of OSA. Consequently an accurate pressure prediction at the level of p_1 is least critical.

The present study experimentally confirms the numerical study reported in (SHOME et al. 1998) for a rigid pharyngeal geometry and in particular the crucial effects of geometrical changes in the morphology. The minimum aperture or the degree of obstruction on the pressure drop is systematically varied in order to explore the influence of small geometrical changes as e.g. caused by surgery. In addition, the applied 'in-vitro' methodology allows validation of major theoretical hypothesis and quantification of the flow model performance. Since measuring flow characteristics and hence theoretical model validation inside an oscillating elastic tube is a difficult task, the presented study is a necessary step towards flow modeling in case of a non-rigid collapsible replica. Experimental validation under controlled and measurable experimental conditions on a non-rigid elastic replica is the next crucial step before extending the findings to a true human pharynx and prediction of surgical interventions.

6. Conclusion

As a first step towards the physical modelling of obstructive sleep apnea, some flow assumptions and resulting flow predictions are experimentally and quantitatively assessed. A rigid 'in-vitro' pharyngeal tongue replica was developed in order to study the flow through a characteristic asymmetrical constriction.

It is shown from a dimensionless analysis that, in first approximation, the fluid flow through the 'in-vitro' replica can be described as steady and incompressible. Measured velocity profiles and measured pressures at different places along the converging part of the constriction confirmed the relevance of a bidimensionnal flow description whereas the viscous pressure losses can be neglected outside the boundary layer. Furthermore the velocity profiles reveal an asymmetry of the flow downstream of the constriction due to the geometrical asymmetry. However transversal pressure measurements on both sides of the constriction show that the influence of the asymmetry on the measured pressure within the constriction is negligible. This point is further confirmed by considering the predictions obtained by a two dimensional flow description from the boundary layer solution and Reduced Navier Stokes simulations. The use of these two dimenstional flow descriptions result in a physical prediction of the position of flow separation.

It is found that the general behaviour of the 'in-vitro' model is different from the classical Starling resistor (LAMBERT and WILSON 1972). As a matter of fact, the outcome of a classical one dimensional flow description is sufficient in applications where only prediction of the volume flow is strived, but fails to predict the pressure distribution. Therefore the one dimensional flow description is not suitable to describe the forces acted by the flow on surrounding structures which is aimed when considering obstructive sleep apnea. Quantitative experimental validation shows that both for the bulk velocity as for the pressure distribution two dimensional flow descriptions yield pressure predictions within an accuracy of 15%. Application of the Reduced Navier Stokes equations are slightly favored since they allow to account for the asymmetry in the geometry.

Further work is needed to evaluate theoretically and experimentally unsteady effects due to flow fluctuation or wall deformation.

Acknowledgment

The authors would like to thank Pierre Chardon, Franz Chouly, Yohan Payan and two anonymous reviewers for their valuable contributions and comments. The work is part of an Emergence project granted by the CNRS federations ELESA/IMAG and the Rhône-Alpes region, France.

REFERENCES

AYAPPA, I. and RAPOPORT, D. (2003), 'The upper airway in sleep: physiology of the pharynx', *Sleep Medicine Reviews* **7**(1), 9–33.

BLEVINS, R. (1992), *Applied Fluid dynamics handbook*, Krieger publishing company, Malabar.

BRIDGMAN, S. and DUNN, K. (2002), 'Surgery for obstructive sleep apnoea', *Cochrane Database Syst Rev* **2**, CD001004.

DEVERGE, M., PELORSON, X., VILAIN, C., LAGREE, P., CHENTOUF, F., WILLEMS, J. and HIRSCHBERG, A. (2003), 'Influence of collision on the flow through in-vitro rigid models of the vocal folds', *J. Acoust. Soc. Am.* **114**(6), 1–9.

FISHMAN, A., MACKLEM, P., MEAD, J. and GEIGER, S. (1986), *The respiratory system. In Handbook of physiology*, Am. Phys. Soc., Maryland.

FLEMONS, W. (2002), 'Obstructive sleep apnea', *New England J. of Medicine* **347**(7), 498–504.

FLEMONS, W. and REIMER, M. (2002), 'Measurement properties of the calgary sleep apnea quality of life index', *Am. J. Respir. Crit. Care Med.* **165**, 159–164.

GROTBERG, J. and JENSEN, O. (2004), 'Biofluid mechanics in flexible tubes', *Annu. Rev. Fluid Mech.* **36**, 121–147.

HENKE, K. (1998), 'Upper airway muscle activity and upper airway resistance in young adults during sleep', *J. Appl. Physiol.* **84**(2), 486–491.

HOFMANS, G., GROOT, G., RANUCCI, M. and GRAZIANI, G. (2003), 'Unsteady flow through in-vitro models of the glottis', *J. Acoust. Soc. Am.* **113**(3), 1658–1675.

HUI, D., CHOY, D., KO, F., LI, T. and LAI, C. (2000), 'Obstructive sleep apnoea syndrome: treatment update', *Medical practice* **6**(2), 209–217.

LAMBERT, K. and WILSON, T. (1972), 'Flow limitation in a collapsible tube', *J of Applied Physiology* **33**, 150–153.

LEITH, D. (1995), 'Cough', *European Respiratory Journal* **8**, 1993–1202.

LIPTON, A. and GOZAL, D. (2003), 'Treatment of obstructive sleep apnea in children : do we really know how ?', *Sleep Medicine Reviews* **7**(1), 61–80.

MANSOUR, K., ROWLEY, J., MESHENISH, A., SHKOUKANI, M. and BADR, M. (2002), 'A mathematical model to detect inspiratory flow limitation during sleep', *J. Appl. Physiol.* **93**, 1084–1092.

MATSUZAKI, Y. and FUNG, Y. (1976), 'On separation of a divergent flow at moderate reynolds numbers', *ASME J Appl Mech* **43**, 227–231.

MAYER, P., PEPIN, J., BETTEGA, G., VEALE, D., FERRETI, G., DESCHAUX, C. and LEVY, P. (1996), 'Relationship between body mass index, age and upper airway measurements in snorers and sleep apnea patients', *Eur Respir J* **9**, 1801–1809.

MCNICHOLAS, W. (2003), 'Sleep apnoea syndrome today: much done, more to do', *Sleep Medicine Reviews* **7**(1), 1087–1093.

PAYAN, Y., CHABANAS, M., PELORSON, X., VILAIN, C., LEVY, P., LUBOZ, V. and PERRIER, P. (2002), 'Biomechanical models to simulate consequences of maxillofacial surgery', *C. R. Biologies* **325**, 407–417.

PEDLEY, T. and LUO, X. (1998), 'Modelling flow and oscillations in collapsible tubes', *J. of Theor. and Comp. Fluid Dyn* **10**, 277–294.

PELORSON, X., HIRSCHBERG, A., HASSELT, R. V., WIJNANDS, A. and AURE-

GAN, Y. (1994), 'Theoretical and experimental study of quasisteady-flow separation within the glottis during phonation. application to a modified two-mass model.', *J. Acoust. Soc. Am.* **96**(6), 3416–3431.

PENZEL, T., MCNAMES, J., de CHAZAL, P., RAYMOND, B., MURRAY, A. and MOODY, G. (2002), 'Systematic comparison of different algorithms for apnoea detection based on electrocardiogram recordings', *Medical & Biological Engineering & Computing* **40**, 402–407.

PEPPARD, P., YOUNG, T., PALTA, M. and SKATRUD, J. (2000), 'Prospective study of the association between sleep-disordered breathing and hypertension', *New England J. of Medicine* **342**(19), 1378–1374.

RAMA, A., TEKWANT, S. and KUSHIDA, C. (2002), 'Sites of obstruction in obstructive sleep apnea', *Chest* **122**(4), 1139–1147.

SCHLICHTING, H. and GERSTEN, K. (2000), *Boundary layer theory*, Springer Verlag, Berlin.

SCHWAB, R., GEFTER, W., HOFFMAN, E., GUPTA, K. and PACK, A. (1990), 'Dynamic upper airway imaging during awake respiration in normal subjects and patients with sleep disordered breathing', *Am J Respir Crit Care Med* **148**, 1385–1400.

SHER, A., SCHECHTMAN, K. and PICCIRILLO, J. (1996), 'The efficacy of surgical modifications of the upper airway in adults with obstructive sleep apnea syndrome', *Sleep* **19**, 156–177.

SHOME, B., WANG, L., SANTARE, M., PRASAD, A., SZERI, A. and ROBERTS, D. (1998), 'Modeling of airflow in the pharynx with application to sleep apnea', *J. of biomechanical engineering* **120**, 416–422.

TERAN-SANTOS, J., JIMINEZ-GOMEZ, A. and CORDERO-GUEVARA, J. (1999), 'The association between sleep apnea and the risk of traffic accidents', *New England J. of Medicine* **340**(11), 847–851.

YOUNG, T., PALTA, M., DEMPSEY, J., SKATRUD, J., WEBER, S. and BADR, S. (1993), 'The occurrence of sleep-disordered breathing among middle-aged adults', *New England J. of Medicine* **17**(328), 1230–1235.

List of Tables

1 Characteristic conditions during obstructive sleep apnea. (*) Estimated from typical volume flow velocity of 30 $\mathrm{l.min}^{-1}$. 31

2 Overall Thwaites and RNSP prediction performance of steady pressure measurements at positions p_1, p_2 and p_3 averaged for all assessed minimum apertures $h_{min} = 1.45mm$, $h_{min} = 1.90mm$, $h_{min} = 2.30mm$ and $h_{min} = 3.00mm$ and indicated ranges of volume flow velocity. 32

TABLES

Table 1
Characteristic conditions during obstructive sleep apnea. (*) Estimated from typical volume flow velocity of 30 $l.min^{-1}$.

L_0	tongue length	5 cm
W_0	pharyngeal width	3 cm
h_0	minimum aperture	2 mm
c_0	speed of sound	350 $m.s^{-1}$
ρ_0	mean density	1.2 kg.m^{-3}
μ_0	dynamic viscosity	1.5 10^{-5} $m^2.s^{-1}$
t_0	period of breathing (inspiratory)	4 s
U_0	flow velocity(*)	8 $m.s^{-1}$

Table 2
Overall Thwaites and RNSP prediction performance of steady pressure measurements at positions p_1, p_2 and p_3 averaged for all assessed minimum apertures $h_{min} = 1.45mm$, $h_{min} = 1.90mm$, $h_{min} = 2.30mm$ and $h_{min} = 3.00mm$ and indicated ranges of volume flow velocity.

ϕ [l/min], Re [-], R^2 [-]	R^2 for p_1	R^2 for p_2	R^2 for p_3
$\phi \leq 120$ (Re ≤ 4719)			
Thwaites	0.48	0.68	0.99
RNSP	0.50	0.71	0.97
$\phi \leq 100$ (Re ≤ 3140)			
Thwaites	0.48	0.69	0.98
RNSP	0.52	0.71	0.97
$\phi \leq 80$ (Re ≤ 2510)			
Thwaites	0.48	0.74	0.99
RNSP	0.57	0.77	0.97
$\phi \leq 60$ (Re ≤ 1888)			
Thwaites	0.48	0.76	0.99
RNSP	0.61	0.82	0.98
$\phi \leq 30$ (Re ≤ 940)			
Thwaites	0.53	0.80	0.99
RNSP	0.72	0.86	0.98

List of Figures

1 Photograph of the in-vitro pharyngeal tongue replica, mounted pressure transducers and hot film. 37

2 Schematic overview of the in-vitro pharyngeal tongue replica, mounted pressure transducers and hot film. The pharyngeal cavity geometry is represented by a flat bottom plate corresponding to y=0 and half cylinders with diameter d=49mm for the assessed h_{min}'s (1.45, 1.90, 2.30 and 3.00mm). The y-axis corresponds with the distance between the flat plate and the half cylinder. The x-axis presents the distance along the longitudinal axis of the replica. The sensor sites are indicated with a solid blue line. The direction of incoming airflow is indicated with an arrow. 38

3 Normalized horizontal velocity profile (0 up to 30mm and 30 down to 0mm) for $h_{min} = 2.3mm$ and a steady flow of 60 l/min. 39

4 Measured vertical (along the y-axis) velocity profile at y=9mm for given flow velocities ϕ with $h_{min} = 2.30$mm. Note the asymmetrical behaviour for ϕ=100 l/min. 40

5 Pressure measurements at p_1, p_2 and p_3 normalized with the upstream pressure p_0 for $h_{min} = 3.00mm$. Pressures are measured on the half cylinder (+) and on the flat bottom plate (o). 41

6 Measured bidimensional velocity profile (absolute value) illustrating flow separation and jet formation along the diverging part of the replica for a steady flow of 40 l/min and $h_{min} = 3.00$mm. A step of $\Delta x = 1$mm in the x direction and $\Delta y = 0.05$mm in the y direction is applied. 42

7 Pressure measurements along the half cylinder at p_1, p_2 and p_3 (+) and Bernoulli simulations with c=1.05 (full line on top) and c=1.2 (full line below) normalised with the upstream pressure p_0 for $h_{min} = 1.45$mm and ϕ=5l/min up to ϕ=120l/min. 43

8 Longitudinal velocity profile with a step of $\Delta x = 1.0$mm for $h_{min} = 3.00mm$ and ϕ=40l/min: measured data (+), Thwaites (▷) and RNSP (x). 44

9 c [-] as function of ϕ predicted from Thwaites (▷), RNSP (x) and the ad hoc constant c=1.05 (full line) for $h_{min} = 1.45mm$. 45

10 Normalized pressure at position p_1 for $h_{min} = 1.45mm$: measured data (+), Thwaites (▷) and RNSP (x). 46

11 Normalized pressure at position p_2 for $h_{min} = 1.45mm$: measured data (+), Thwaites (▷) and RNSP (x). 47

12 Normalized pressure position p_3 for $h_{min} = 1.45mm$: measured data (+), Thwaites (▷) and RNSP (x). 48

13 Normalized pressure at position p_1 for $h_{min} = 3.00mm$: measured data (+), Thwaites (▷) and RNSP (x). 49

14 Normalized pressure at position p_2 for $h_{min} = 3.00mm$: measured data (+), Thwaites (▷) and RNSP (x). 50

15 Normalized pressure at position p_3 for $h_{min} = 3.00mm$: measured data (+), Thwaites (▷) and RNSP (x). 51

FIGURES

Figure 1. Photograph of the in-vitro pharyngeal tongue replica, mounted pressure transducers and hot film.

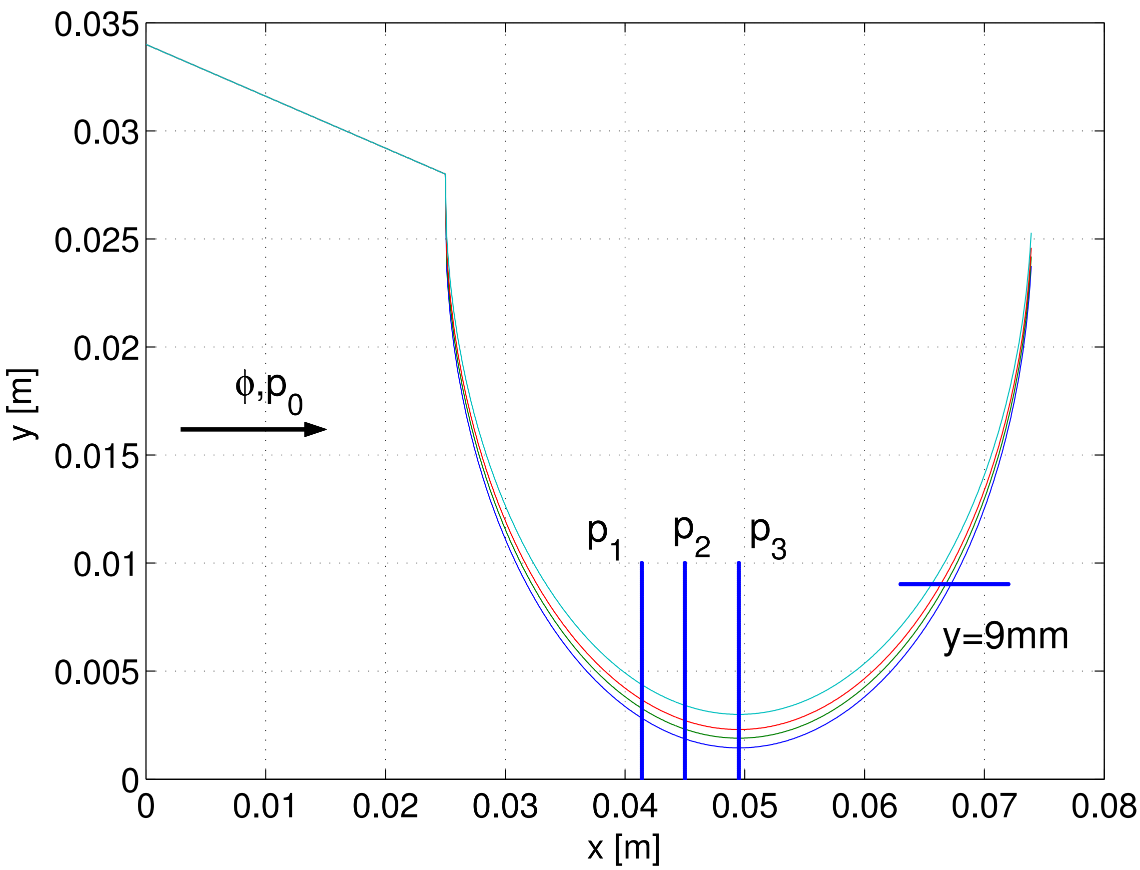

Figure 2. Schematic overview of the in-vitro pharyngeal tongue replica, mounted pressure transducers and hot film. The pharyngeal cavity geometry is represented by a flat bottom plate corresponding to y=0 and half cylinders with diameter d=49mm for the assessed h_{min}'s (1.45, 1.90, 2.30 and 3.00mm). The y-axis corresponds with the distance between the flat plate and the half cylinder. The x-axis presents the distance along the longitudinal axis of the replica. The sensor sites are indicated with a solid blue line. The direction of incoming airflow is indicated with an arrow.

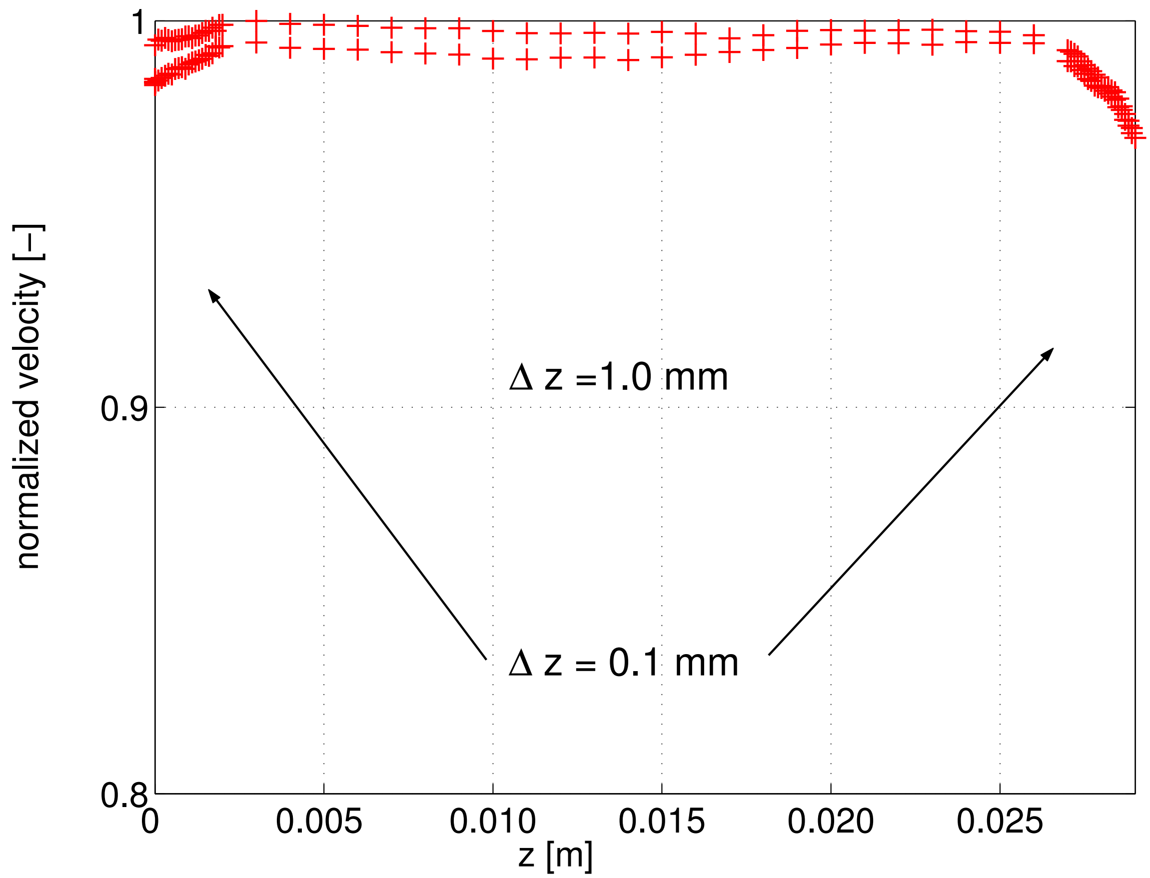

Figure 3. Normalized horizontal velocity profile (0 up to 30mm and 30 down to 0mm) for $h_{min} = 2.3mm$ and a steady flow of 60 l/min.

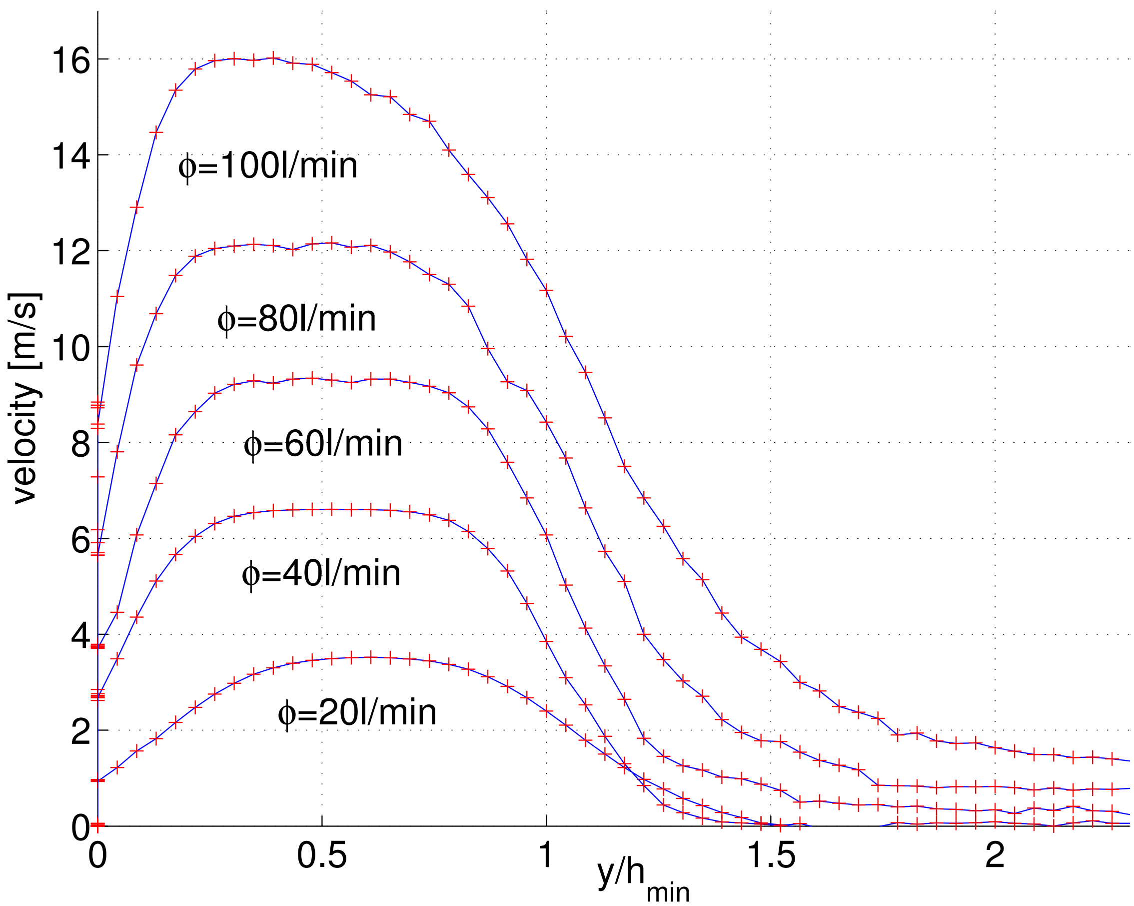

Figure 4. Measured vertical (along the y-axis) velocity profile at y=9mm for given flow velocities ϕ with $h_{min} = 2.30$mm. Note the asymmetrical behaviour for ϕ=100 l/min.

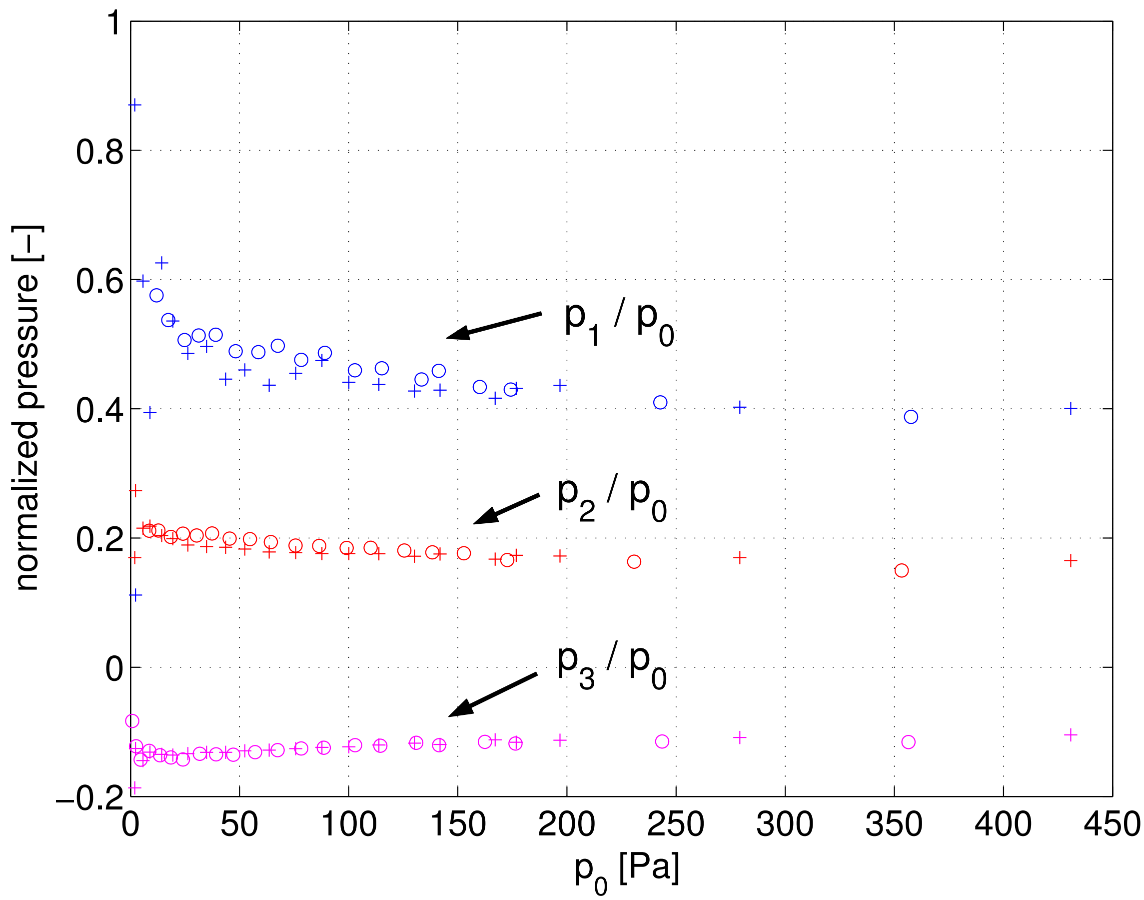

Figure 5. Pressure measurements at p_1, p_2 and p_3 normalized with the upstream pressure p_0 for $h_{min} = 3.00mm$. Pressures are measured on the half cylinder (+) and on the flat bottom plate (o).

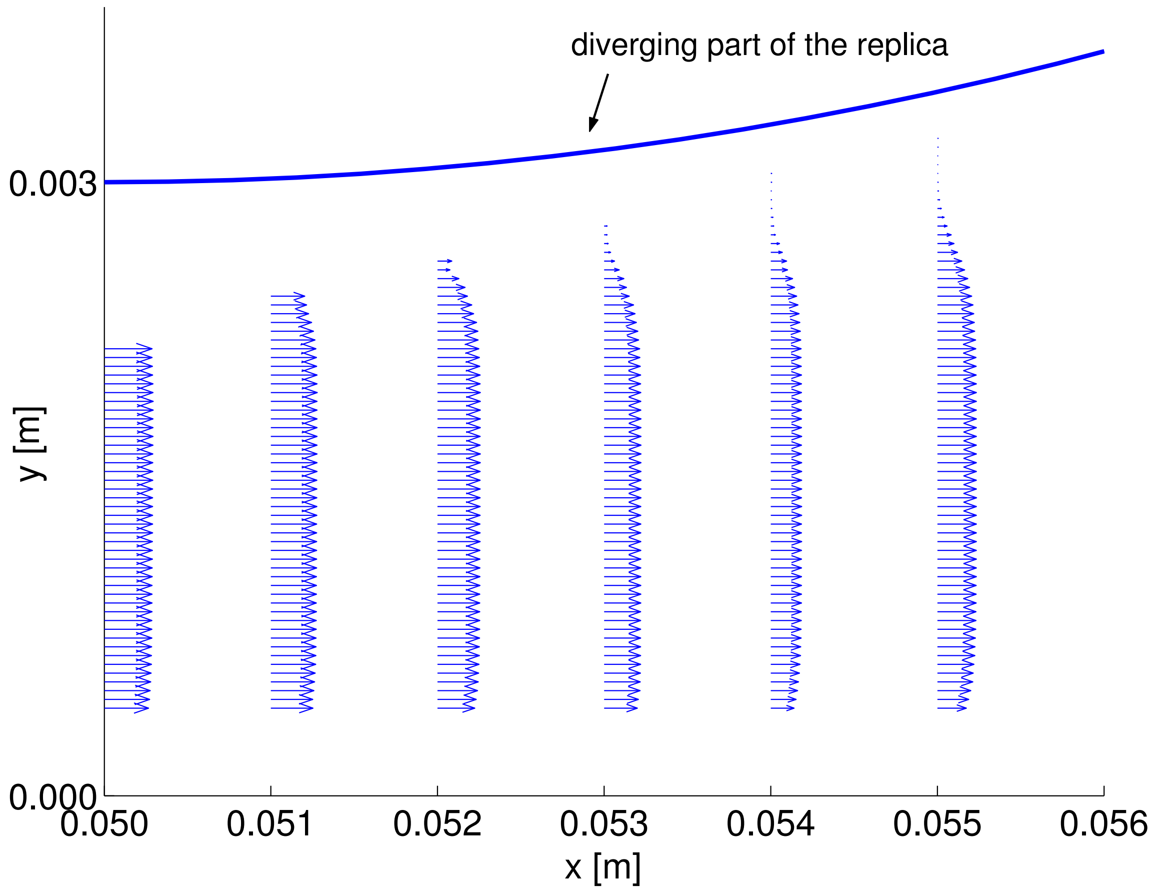

Figure 6. Measured bidimensional velocity profile (absolute value) illustrating flow separation and jet formation along the diverging part of the replica for a steady flow of 40 l/min and $h_{min} = 3.00$mm. A step of $\Delta x = 1$mm in the x direction and $\Delta y = 0.05$mm in the y direction is applied.

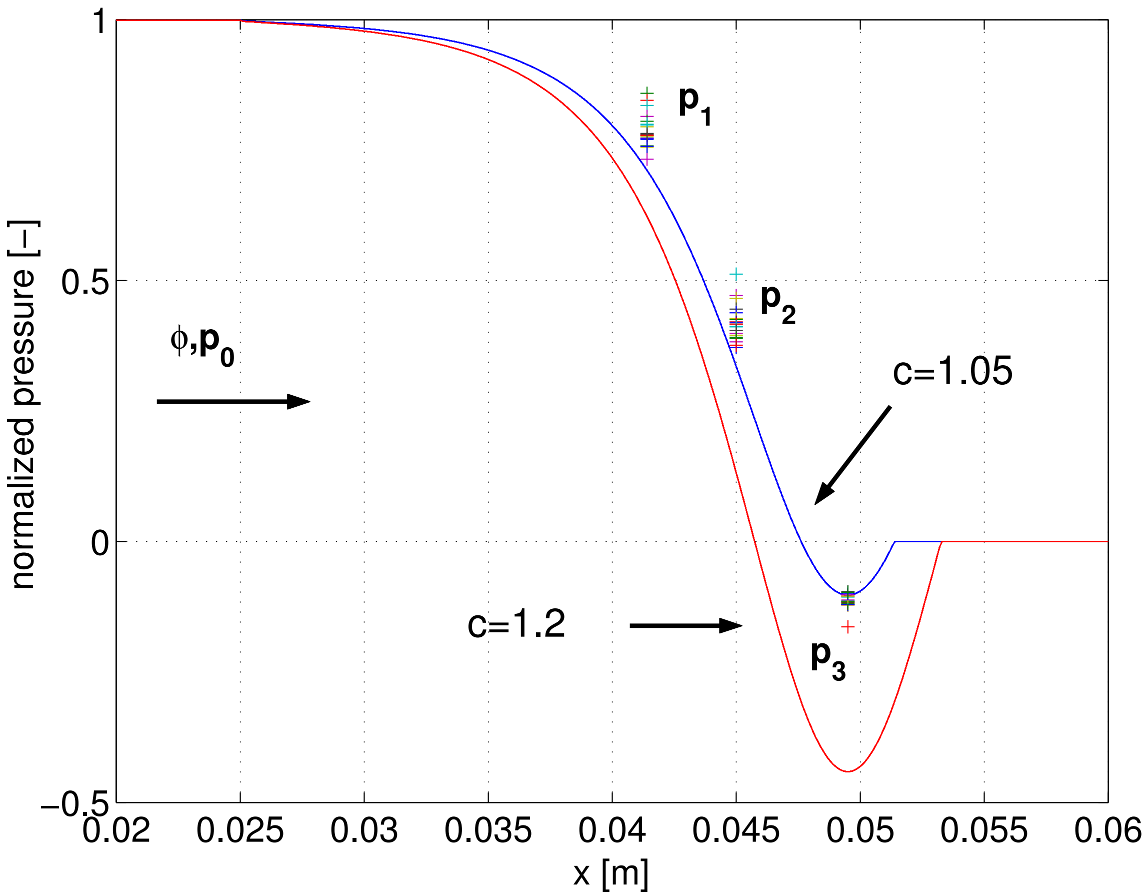

Figure 7. Pressure measurements along the half cylinder at p_1, p_2 and p_3 (+) and Bernoulli simulations with c=1.05 (full line on top) and c=1.2 (full line below) normalised with the upstream pressure p_0 for $h_{min} = 1.45$mm and ϕ=5l/min up to ϕ=120l/min.

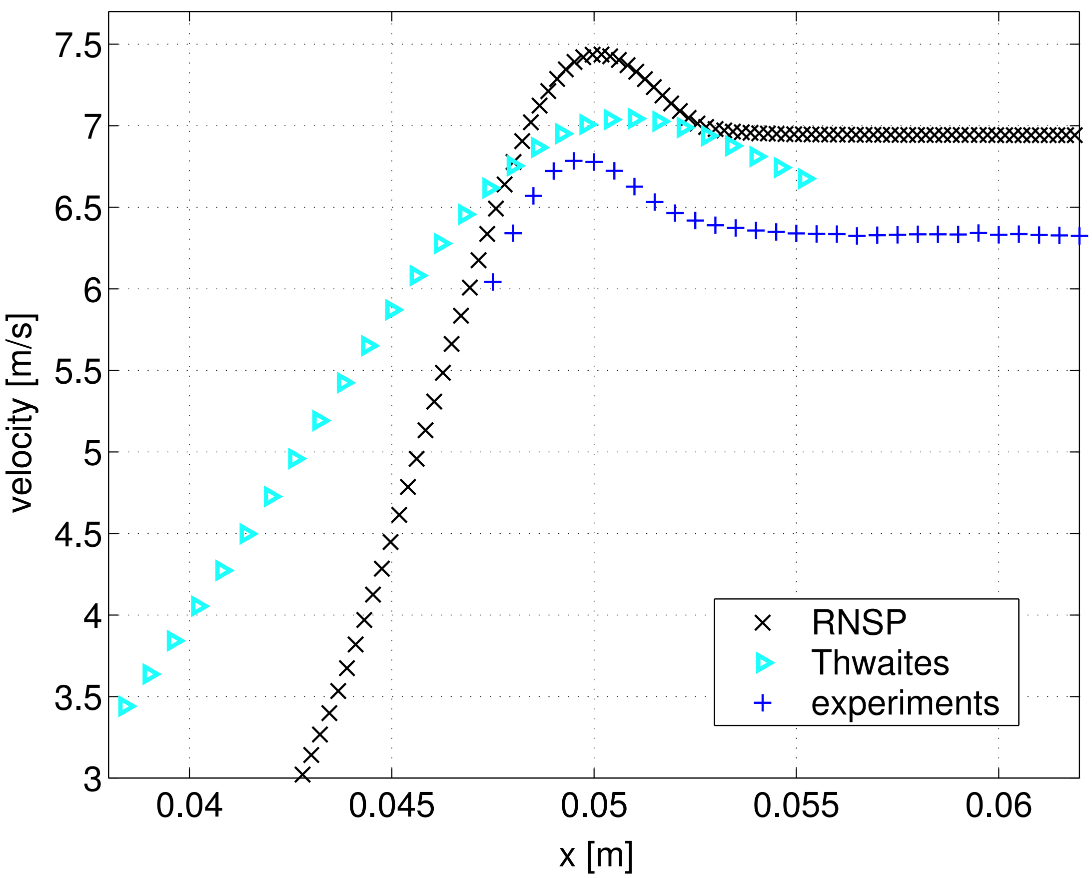

Figure 8. Longitudinal velocity profile with a step of Δx = 1.0mm for $h_{min} = 3.00mm$ and ϕ=40l/min: measured data (+), Thwaites (▷) and RNSP (x).

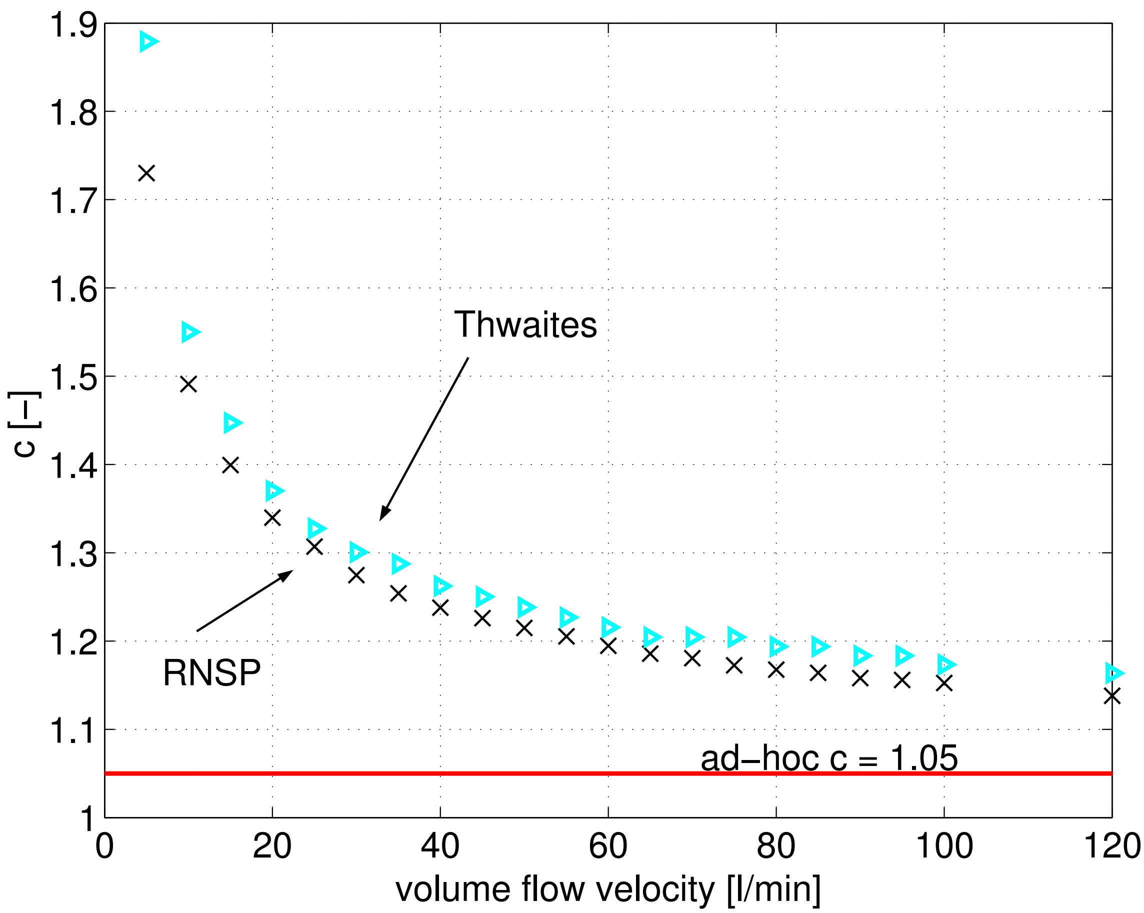

Figure 9. c [-] as function of ϕ predicted from Thwaites ($\triangleright$), RNSP (x) and the ad hoc constant c=1.05 (full line) for $h_{min} = 1.45mm$.

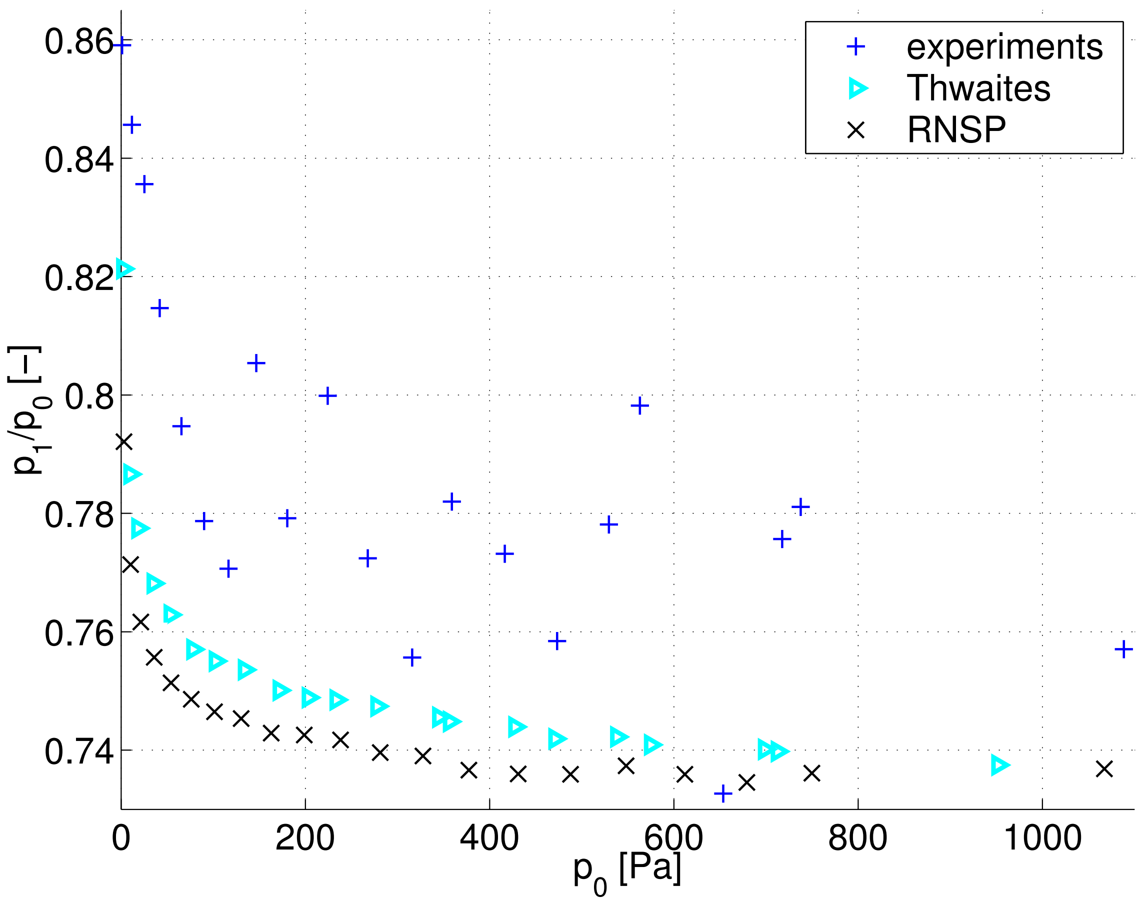

Figure 10. Normalized pressure at position p_1 for $h_{min} = 1.45mm$: measured data (+), Thwaites (▷) and RNSP (x).

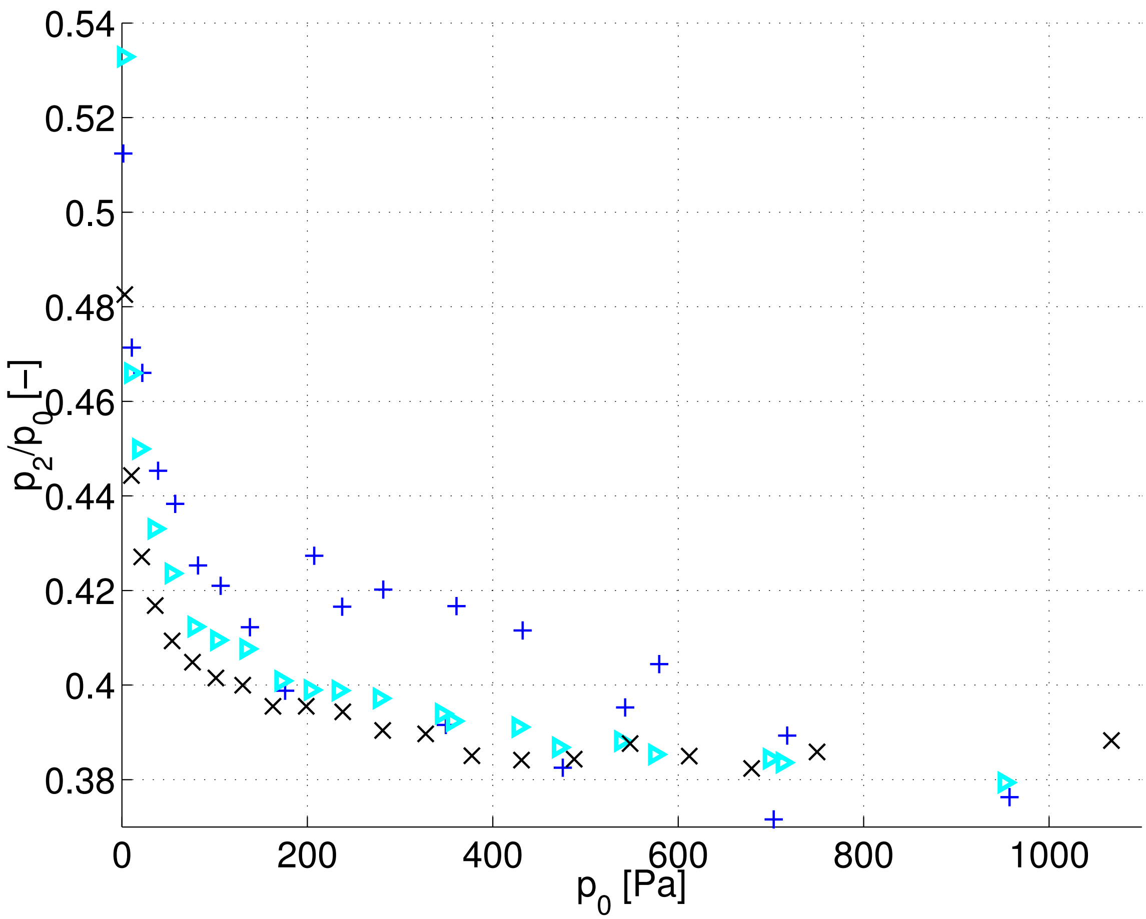

Figure 11. Normalized pressure at position p_2 for $h_{min} = 1.45mm$: measured data (+), Thwaites (▷) and RNSP (x).

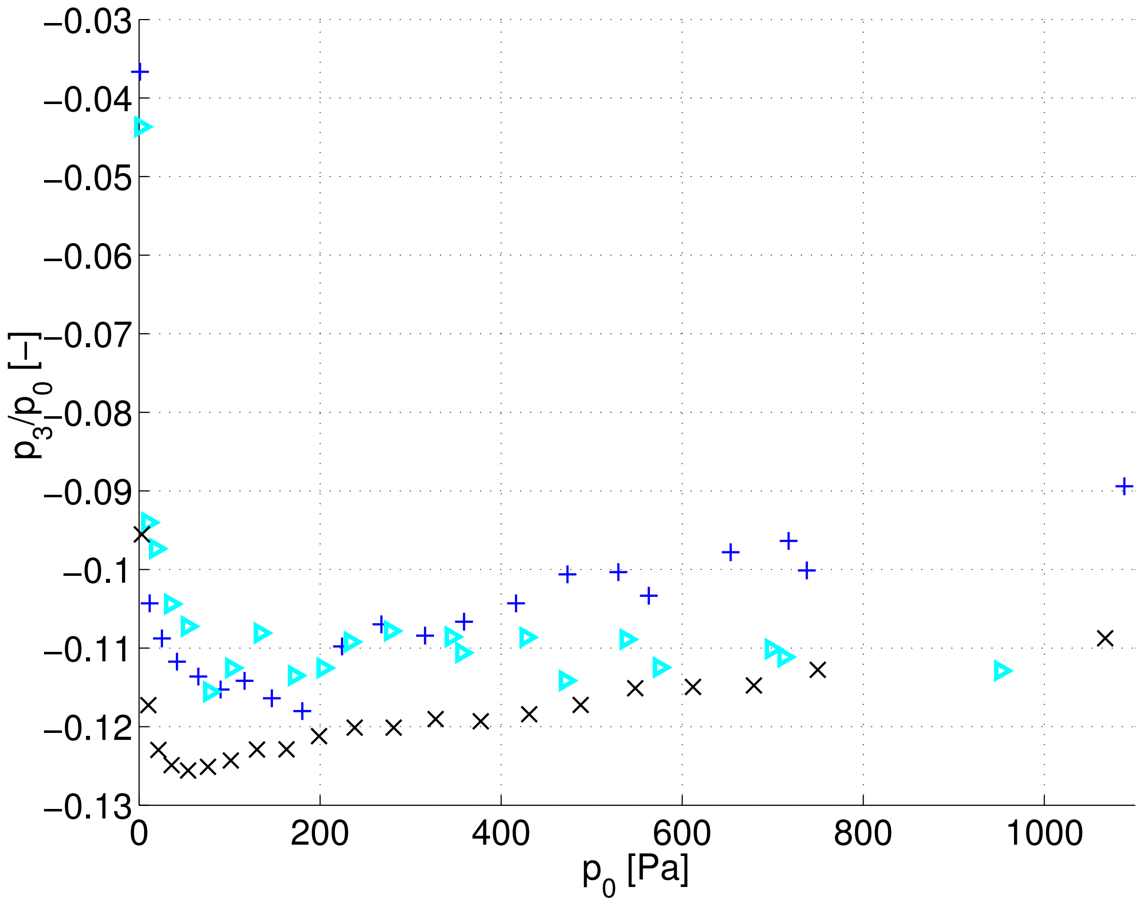

Figure 12. Normalized pressure position p_3 for $h_{min} = 1.45mm$: measured data (+), Thwaites (▹) and RNSP (x).

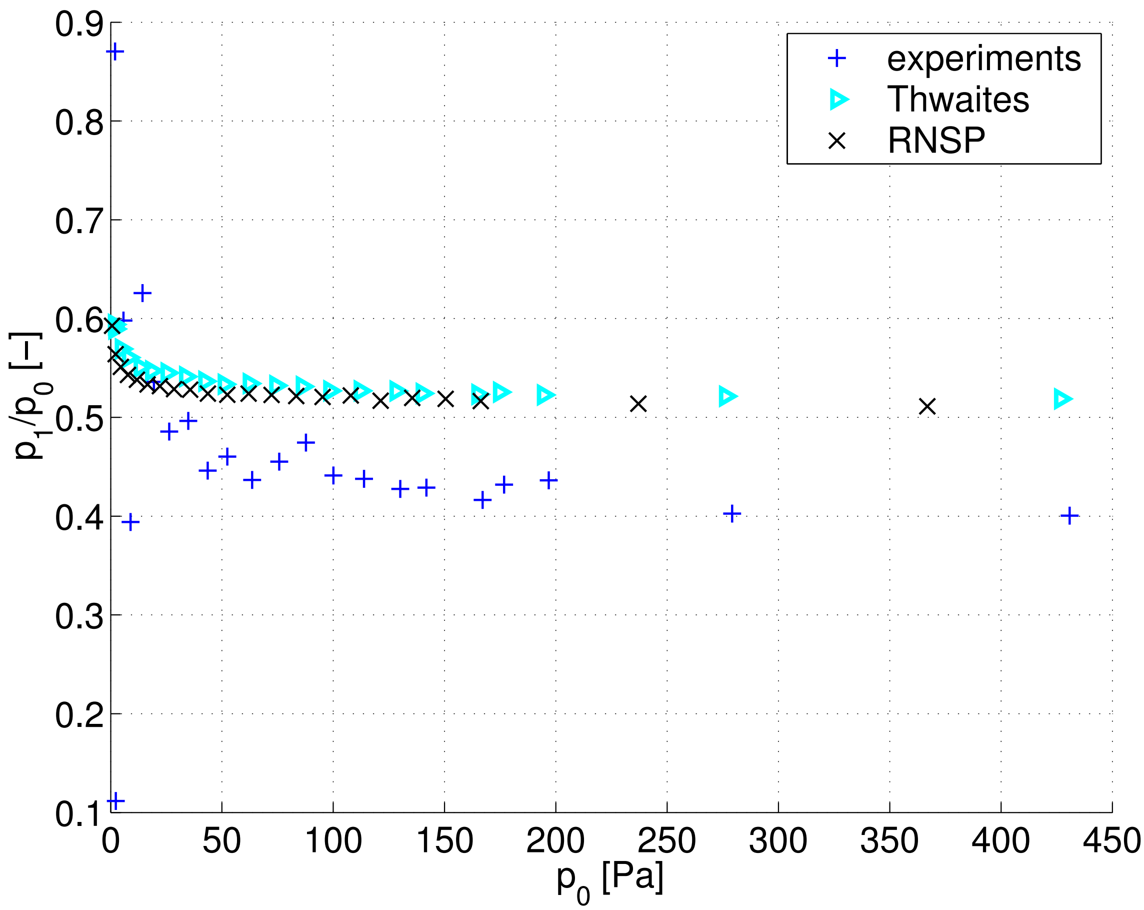

Figure 13. Normalized pressure at position p_1 for $h_{min} = 3.00mm$: measured data (+), Thwaites (▷) and RNSP (x).

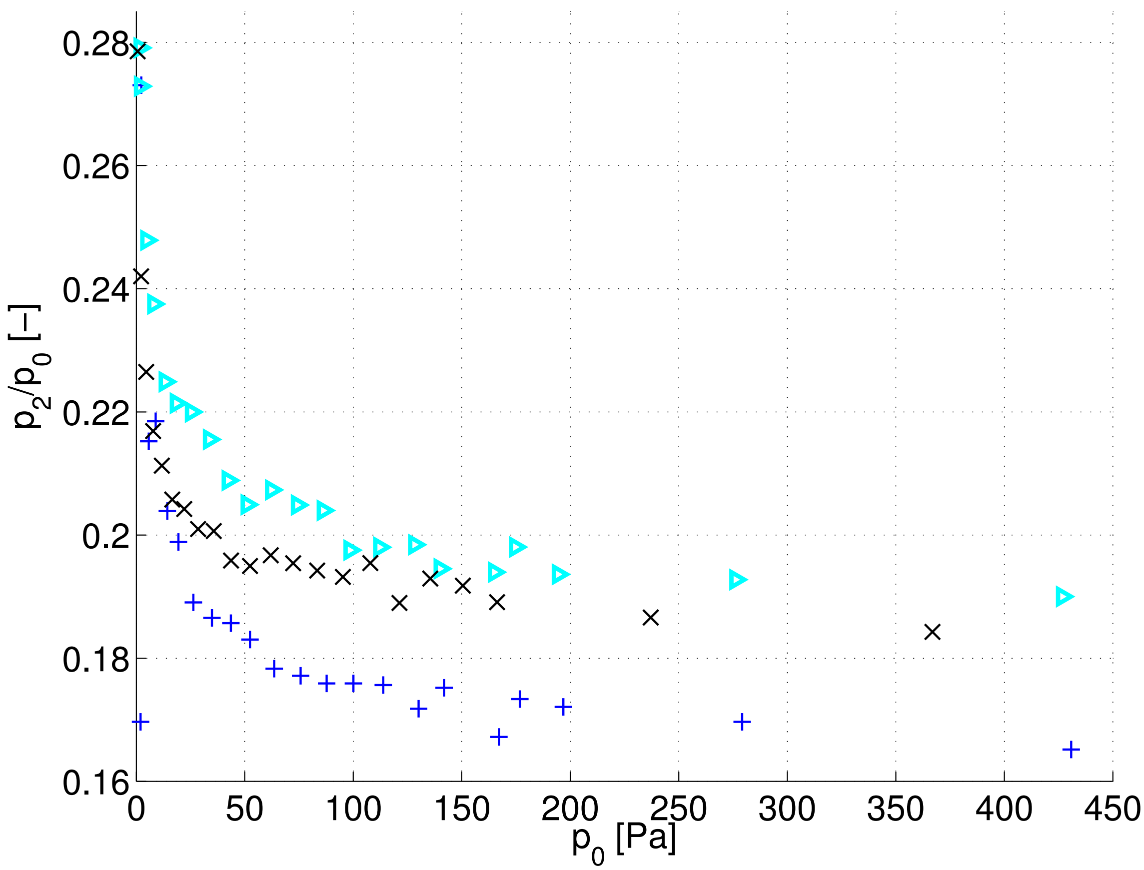

Figure 14. Normalized pressure at position p_2 for $h_{min} = 3.00mm$: measured data (+), Thwaites (▷) and RNSP (x).

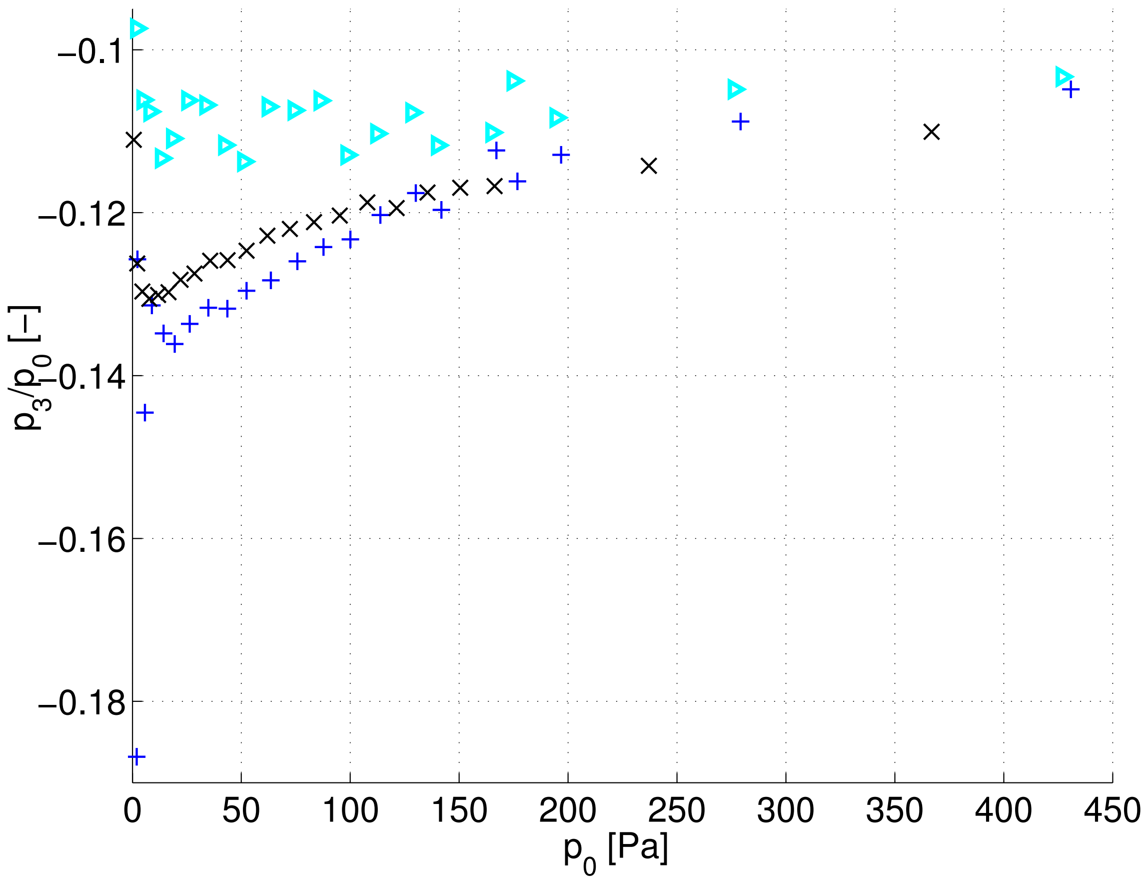

Figure 15. Normalized pressure at position p_3 for $h_{min} = 3.00mm$: measured data (+), Thwaites (▷) and RNSP (x).

Biograhpy